Optics Communications 281 (2008) 4788–4792

Contents lists available at ScienceDirect

Optics Communications

journal homepage: www.elsevier.com/locate/optcom

Resolution improvement of surface plasmon-enhanced, liquid crystal spatial light modulator: Simulation studies

P. Kogan [a], B. Apter [b], I. Baal-Zedaka [b], U. Efron [a,b,*]

[a] Department of Electro-Optical Engineering, Ben-Gurion University of the Negev, Beer-Sheva 84105, Israel
[b] Department of Electrical and Electronic Engineering, Holon Institute of Technology, Holon, Israel

ARTICLE INFO

Article history:
Received 21 February 2008
Received in revised form 22 May 2008
Accepted 4 June 2008

PACS:
42.25.Fx
73.20.Mf
42.70.Df
42.30.Lr

Keywords:
Surface plasmon resonance
Spatial light modulator
Liquid crystal
Spatial resolution

ABSTRACT

Spatial resolution is an important performance characteristic of spatial light modulators (SLM). One of the key factors affecting the spatial resolution of liquid crystal (LC)-based SLM is the fringing field effect. This effect can be reduced in thin LC cells with corresponding reduction in the electro-optical response. A strong electro-optic response in thin LC layer can be attained using the surface plasmon resonance (SPR) phenomenon. While SPR-based LC SLMs were already demonstrated about 15 years ago, their development has been hampered in part by low resolution, due to the finite propagation length of the surface plasmons (SPs). A fine patterning of the metal layer supporting the propagation of SPs is studied as a possible solution for reducing the spatial blurring associated with the long propagation length of SPs. The results of detailed computer simulations showing improved resolution SPR-LC–SLM are presented.

1. Introduction

Surface plasmons (SPs) have been extensively studied over the past years [1–3]. They are highly sensitive to minute changes in the dielectric properties of the constituting materials. Novel device applications, based on surface plasmon resonance (SPR) were recently developed and demonstrated. Among them are sensors and biosensors [4–9], surface plasmon microscopy (SPM) [10–17] and spatial light modulators (SLMs) [18–22]. While much advance has been made in the areas of sensors, biosensors and microscopy, little progress has been reported in SPR-based SLMs, since the beginning 1990's when such devices were first demonstrated. In these devices the optical-active material was either a LC [20] or an electro-optic polymer [22].

By using the SPR effect, an enhanced electro-optic response in thin LC layer can be attained. The application of thin LC layer allows reducing the fringing field effect [23–25] which limits the spatial resolution of conventional LC-based SLMs. These devices employ a relatively thick LC layer in order to attain adequate electro-optical response. On the other hand the spatial resolution of the thin LC, SPR-based SLMs is limited by the finite propagation length (several tens of micrometers) of the SPs [20]. The same limitation also exists in SPM [13]. Among the few attempts that have been made to improve the spatial resolution in SPM are the variations of the imaging wavelength [12], usage of defocused high-numerical-aperture liquid-immersion objectives [15] and operating at different SPR angles by rotating the object [16]. None of these techniques is suitable for an SLM application.

The present study is aimed at improving the spatial resolution of the SPR-based SLM by optimizing the metal-dielectric structure of the device. To this end we simulated the use of fine patterning of the metal layer supporting the propagation of SPs, instead of a continuous one, which has been used in previous studies of SLM structures. Such patterned structure alters locally the SP's fields, resulting in the reduction of the propagation length. This concept has been studied by computer simulation of spatial light modulation performance. In our simulations we used the following commercially available software: (a) RCWA-based GSOLVER program [26] and (b) FDTD-based OptiFDTD program [27] for simulation of the SP's excitation and propagation. A third, commercially available software, Autronics-Melchers 2dimMOS program [28], was used for the simulation of the LC behavior.

* Corresponding author. Address: Department of Electro-Optical Engineering, Ben-Gurion University of the Negev, Beer-Sheva 84105, Israel. Tel.: +972 8 647 9805; fax: +972 8 647 9494.
E-mail address: efron@bgu.ac.il (U. Efron).

0030-4018/$ - see front matter © 2008 Elsevier B.V. All rights reserved.
doi:10.1016/j.optcom.2008.06.003

2. SPR-based SLM

Surface plasmons are electromagnetic waves propagating at the interface between a metal and a dielectric, and related to the longitudinal oscillations of free electrons at the metal surface and an evanescent optical wave in the dielectric. It was shown [2] that SPs can only propagate at the interface between materials with opposite signs of dielectric permittivity, such as between a dielectric (positive permittivity) and a metal (negative real part of dielectric permittivity). The polarization of SPs is purely TM (p-polarization), due to the fact that the discontinuity of the electric field component, perpendicular to the metal surface, generates a surface charge density at the interface. The SP fields are evanescent in both materials, with a transverse decay distance of several hundred nanometers in the dielectric and a significantly shorter one in the metal.

An excitation of SPs by a light beam is difficult due to the fact that at a given photon frequency the real part of the SP's wave number is larger than that of the incidence light, or alternatively that the phase velocity of the SP is less than that of light (the angular frequency–momentum (ω–k) dispersion curve of the SP lies to the right of the light line) [2]. In order to excite SPs by light, one has to increase the wave number of the incidence light or slow down its phase velocity. This can be done by allowing the light to pass through a dense medium. Such approach is implemented in the prism coupling, known as attenuated total reflection (ATR) configuration, developed by Kretschman [29]. In this configuration the refractive index of glass prism should be larger than that of the dielectric layer. Also, the metal layer should be relatively thin (about 50 nm). The physical process behind the SP excitation is total internal reflection (TIR) which an incident TM-polarized beam undergoes at the prism base. In this way, the generated evanescent field, extends through the thin metal film and excites the SP at the interface between the metal and the dielectric layer. The excitation of the SP results in a dip in the reflected intensity which occurs as the angle of incidence matching the critical angle. As a result, the incident optical beam, traveling through the bulk of the material, is absorbed by the resonantly excited SPs, which are surface waves. This effect is called "Surface Plasmon Resonance" (SPR). The position, depth, and width of the dip in the reflectivity curve depend strongly on the dielectric permittivity of both the metal and the dielectric, as well as on the thickness of the metal layer.

One can use dielectric materials whose refractive index can be spatially modulated, (e.g. LC), and thus achieve SPR-based spatial light modulation directly by reflection. The attractive features and drawbacks of this concept have been previously described [18,20]. Due to the fact that the switching takes place entirely within the evanescent field region and that the modulated beam does not propagate through the active medium (LC), the thickness of the LC layer can be significantly reduced (<1 μm) compared to that of conventional LC–SLMs. Thus, the fringing field [24] effect can be significantly suppressed.

The drawback of this approach is that the finite plasmon propagation length of SPs results in a blurring effect on the image. Thus, the spatial resolution in the direction of plasmon propagation is limited by the characteristic propagation length [20], which is around 10–20 μm (equivalent to a spatial frequency of 25–50 lp/mm) at a wavelength of 630 nm.

3. Description of the proposed concept

In order to improve the spatial resolution of SPR–LC–SLM, we have studied the use of a periodic, small-scale grooving of the metal layer instead of the use of a continuous one. It is expected that such patterning will reduce the propagation length of the SPs and thus reduce the spatial blurring of modulated image. It was shown in [12], that the spatial resolution of SPM imaging can be improved by using gold layer instead of a silver one. The reason is that the SP propagation length for gold is shorter than that for silver. On the other hand the SPR's optical modulation contrast for gold is lower than that for silver. It is known [20] that the wider the effective width of the SPR dip the shorter the propagation length of SPs. Fig. 1 shows the SPR reflection curves, analytically calculated for silver and gold layers. The solid and dashed curves correspond to the different refractive indexes of the active layer. It is clear that the SPR dip for gold (in an approximate resonance angle of 76°) is much wider than that for silver (approximate resonance angle of 70°). However when the SPR position is changed (dotted curve), the contrast ratio attained for silver is higher than that of gold. Consequently, there exists a clear trade-off between the contrast modulation and the spatial resolution. Apparently, there exists no metal which can simultaneously meet both the high spatial resolution (shorter SP propagation length) and the high contrast requirements.

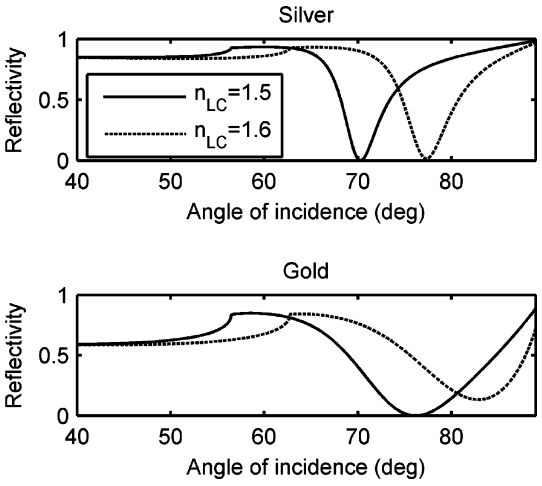

Fig. 1. SPR curves calculated for silver layer (refractive index: $n_{Ag} = 0.143 + 3.787j$, thickness: 46 nm) and for gold layer (refractive index: $n_{Au} = 0.316 + 3.121j$, thickness: 37 nm) in a prism configuration, at a wavelength 630 nm. The refractive index of glass prism is 1.8. The refractive index of the dielectric layer is switched between $n_{LC} = 1.5$ and $n_{LC} = 1.6$.

In this work we tested the assumption that a small-scale patterning (grooving) of the silver layer, can result in a surface, supporting the SPs propagation, with reduced longitudinal decay length, which will allow meeting the simultaneous requirements of high spatial resolution and high contrast.

4. Simulation details and results

The simulations performed for the 2-D SLM device are schematically shown in Fig. 2. The device (taken after the LC SLM configuration described in [18]) is based on a prism-excitation configuration. A thin patterned (grooved) silver layer is deposited on top of the glass prism, followed by the first LC alignment layer. The metal pixel electrodes are deposited on top of the opposing glass plate, followed by the deposition of the second LC alignment layer. The active LC layer is sandwiched between the two alignment layers. The patterned metal layer is characterized by its thickness d_m, patterning pitch Λ and groove width δ. It should be noted that the period of the driving electrodes is larger than the pitch of the patterned metal layer.

Computer simulations were performed for two cases. The first one was a continuous silver layer, $\delta = 0$ (C-structure). The other structure was a patterned (grooved) silver layer with the patterning

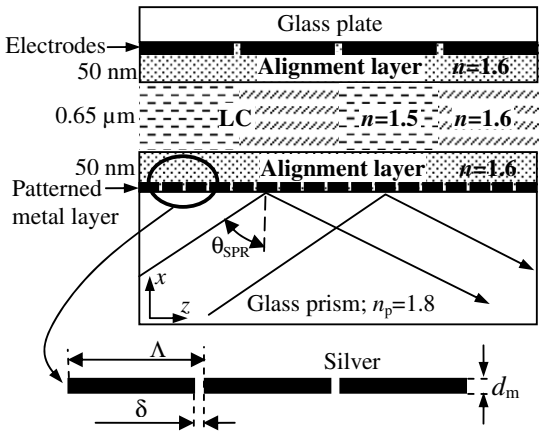

Fig. 2. Schematics of the simulated device.

pitch $\Lambda = 1$ μm and a groove width: $\delta = 0.2$ μm (P-structure). The grooves of the P-structures were filled with a LC alignment material. The refractive index of silver was calculated from the Lorentz-Drude model with parameters from reference [30], which yield, for a wavelength of 630 nm: $n_{Ag} = 0.143 + 3.787j$. The refractive index of the prism is 1.8. The LC thickness was chosen as 0.65 μm, which is larger than the penetration depth of the plasmon's field (in the x-direction), thus allowing the influence of the upper glass plate to be neglected. It should be noted that all simulations were performed for two-dimensional structures.

In the first stage we performed simulations with RCWA, to obtain the required thickness of the silver (d_m) and the angle of the SPR (θ_{res}). Since the GSOLVER program does not enable the simulation of an anisotropic material, the LC layer was taken as an isotropic medium with a variable refractive index changing between its ordinary n_o and extraordinary n_e values. For a typical nematic LC material such as E7, the effective refractive index varies between $n_o = 1.5$ and $n_e = 1.7$. It is assumed that in the initial, non-activated state, the director of the LC layer is aligned parallel to the metal layer, along the z-axis. Thus the SPs will experience an effective refractive index close to the ordinary value n_o. This situation corresponds to the solid SPR curves in Fig. 3. When voltage is applied to the LC layer, the director is reoriented towards the direction perpendicular to the metal layer and the effective refractive index of LC layer is increased. This case corresponds to the dashed curves

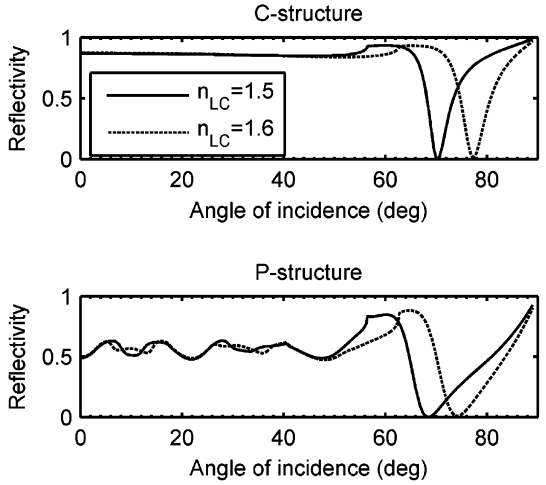

Fig. 3. SPR curves for the two simulated structures (RCWA simulation).

in Fig. 3, where the refractive index of the LC layer is 1.6 (between the n_o and the n_e values).

For all cases, the conditions of the optimal SPR excitation were found by iterative procedure, which involved optimization of the angle of incidence and thickness of the metal layer. The minimum reflectivity value at the resonance angle was chosen as an optimization criterion. The SPR propagation behavior was subsequently computed using the FDTD method. The FDTD simulations were performed with 2D structures, using plane incident wave. The OptiFDTD software allows the computation of near and far field distributions of the SPs and of the reflected, spatially modulated light.

Table 1 presents the optimized values of the metal layer thickness and the resonance angle calculated for the different structures. It can be seen, that the values calculated by the RCWA and FDTD methods for the same structure are very close. When the LC refractive index was changed to 1.6, there was no excitation of SPs (at the same angle of incidence), and almost all of the incident radiation was reflected.

The SLM performance for the various spatial resolutions was simulated with the FDTD software, by introducing a LC layer with a periodically modulated refractive index. The LC layer was simulated with the 2dimMOS software [28] which computes the two-dimensional distribution of the LC director.

We used the elastic and dielectric constants of a typical, positive anisotropy, E-7-like nematic LC (thickness of 0.65 μm), from Ref. [31]. The initial alignment of the LC layer was homogeneous with 2° pre-tilt angle at the boundaries. The two-dimensional spatial distribution of the refractive index of LC, experienced by the SP is determined by the expression [32]

$$n_{LC}(x,z) = \frac{n_e n_o}{\sqrt{n_e^2 \cos^2\theta(x,z) + n_o^2 \sin^2\theta(x,z)}}, \quad (1)$$

where $\theta(x,z)$ is the 2-D distribution of the director tilt angle. The field distributions were computed for modulation periods of 6, 7, 9, 12, 14 and 20 μm. Fig. 4 shows the two-dimensional spatial distributions of the refractive index and the LC director for two spatial modulation periods. The bottom curves in Fig. 4 shows the refractive index profile at a depth of $x = 0.15$ μm, which corresponds to half the penetration depth of the plasmon's intensity in the x-direction.

The effect of the fringing field is clearly seen, as the broadened transitions of the index profile at the 6 μm-modulation period. The transition width is approximately equal to three times the thickness of the LC layer. The spatial distribution of the refractive index presented in Fig. 4 was used for the FDTD simulation of the SPR-based SLM. Fig. 5 shows examples of near field energy distribution (z-component of the Poynting vector) for the two structures, with an index modulation period of 20 μm. Due to the strong enhancement of the SP field near the metal layer, the gray levels of the figures were saturated in order to show the reflected light, whose intensity is much weaker. In the simulations, the plane of the incident field (plane wave) was positioned at $x = -0.375$ μm (dashed straight line), and the metal layer (solid line) at $x = 0$. The interference pattern between the incident and the reflected light can clearly be observed in the region between the metal layer and

Table 1
Metal thicknesses and resonance angles of the SPR for the simulated structures

Structure	Groove width δ (μm)	d_m (nm)		θ_{res} (deg)	
		RCWA	FDTD	RCWA	FDTD
C	0	46	45	70.3	69.3
P	0.2	36	40	67.2	66.5

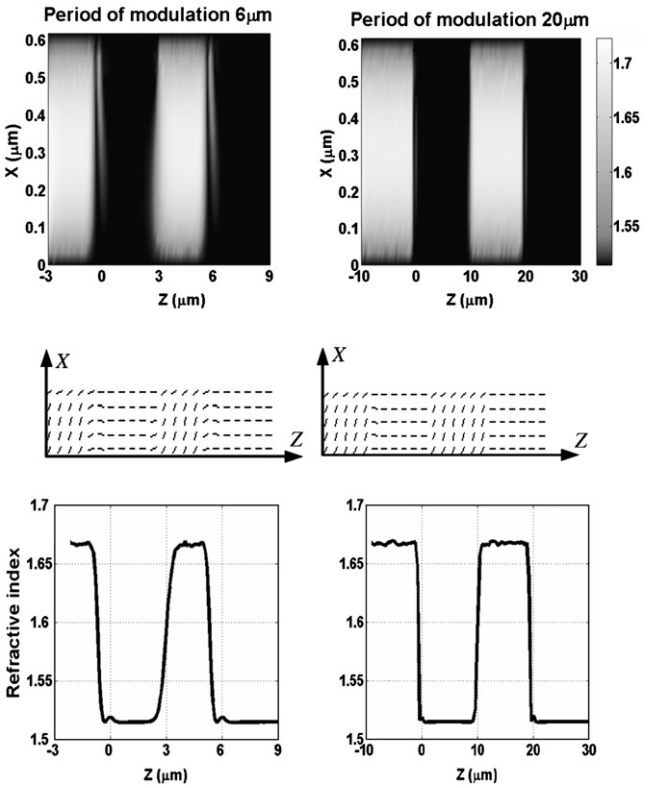

Fig. 4. Two-dimensional distributions of the refractive index of LC (top), LC director (middle) and the refractive index profile at a depth of $x = 0.15$ μm (bottom).

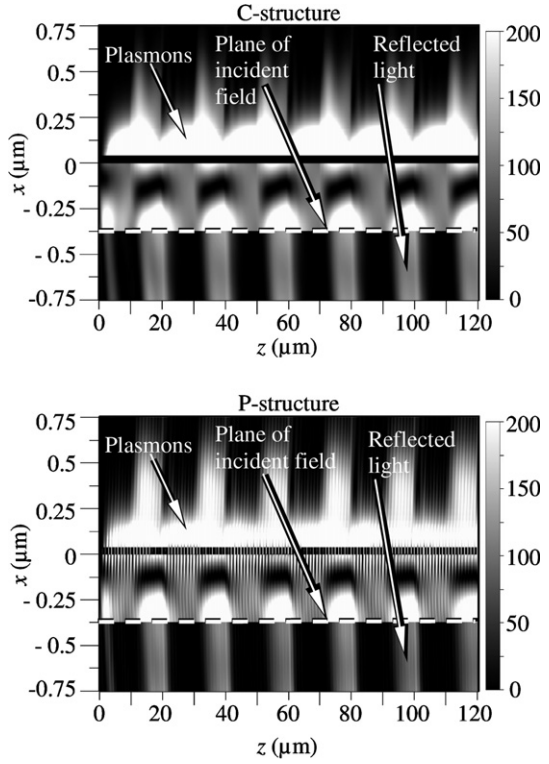

Fig. 5. Two-dimensional distribution of Poynting vector's z-component for the C- and P-structures. The units of the grayscale palette are arbitrary.

the plane of the incident field. The periodic modulation of the reflected light is clearly seen in the region of $x \leqslant -0.375$ μm.

In order to get a more detailed spatial distribution of the reflected light, we calculated the z-component of the Poynting vector at a depth of $x = -0.75$ μm for one period of spatial modulation, which can be seen at the bottom of Fig. 6. The profile of the refractive index is also shown in Fig. 6. It is should be pointed out that the curves at the bottom of Fig. 6 are displaced in the z-direction, relatively to the refractive index profile, due to the oblique angle of incidence (SPR angle), with a lateral shift being: $2 \times 0.75 \times \tan\theta_{SPR}$. Since the simulation was done at a depth of $x = -0.75$ μm, the estimated shift using values from Table 1, comes to 3.5 μm and 4 μm for the P- and C-structures, respectively. Fig. 6 indicates that the use of the P-structure (the patterned metal layer) results in a shorter SP propagation length than that of the C-structure (continuous metal layer).

The near field at the plane $x = -0.75$ μm was used for the calculation of the angular distribution of the diffraction intensity, in the far field. The normalized far field diffraction intensity is shown in Fig. 7. It can be seen from these intensity distributions that for the shorter period (14 μm) the overall intensity of nonzero diffraction orders ($+1R$, $-1R$) for the P-structure is higher by factor of 1.8 than that of the C-structure clearly showing the improvement of spatial resolution.

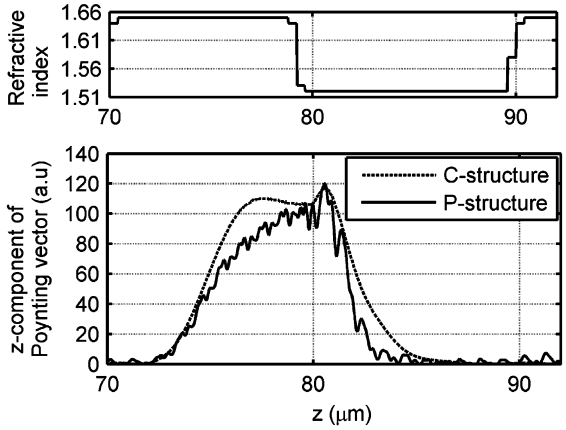

Fig. 6. z-Component of the Poynting vector (bottom) and refractive index profile (top) for one period of spatial modulation.

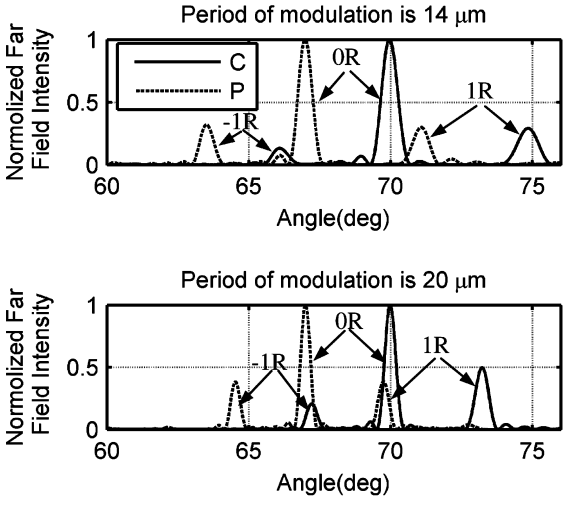

Fig. 7. Normalized far field diffraction intensity for two periods of modulation: 14 μm (top) and 20 μm (bottom). $1R$, $0R$ and $-1R$ are the first, zero and minus one reflected diffraction orders, respectively.

The calculations, whose results are presented in Figs. 5–7 were repeated for six modulation periods between 6 μm and 20 μm, and are given in the form of a modulation transfer function (MTF). This MTF is defined as a sum of the diffracted power at the $1R$ and $-1R$ orders, relative to the zero-order ($0R$) power. The MTFs for the two structures are shown in Fig. 8.

Fig. 8 supports the assumption that patterning of metal layer improves the spatial resolution of SPR-based SLM. At an MTF of 50%, the spatial resolution for the C-structure is about 70 lp/mm while that of P-structure is about 100 lp/mm. At higher spatial frequencies (>80 lp/mm) there is almost a two-fold improvement in the resolution.

A thin LC cell of thickness $d_{cell} = 0.65$ μm was used, in order to reduce the effect of the fringing field. Assuming a fringing field broadening of around $3d_{cell}$ [33] (Fig. 4), i.e. about $\Delta d \sim 2$ μm, the limiting spatial frequency is expected to be around $f_{max} \sim 1/(2\Delta d) \sim 250$ lp/mm or, significantly above the plasmonic limiting frequency of around 170 lp/mm, as observed from Fig. 8.

We attribute the improvement in spatial resolution of the P2-structure to the effective change in the complex refractive index of the patterned metal layer. In order to estimate the effective refractive index of the patterned layer we performed an RCWA simulation aimed at fitting the SPR curve of a structure composed of a continuous layer made of an effective index material, to the SPR curve obtained with our patterned P-structure. This fitting was done by an iterative procedure during which the real and the imaginary parts of refractive index of the effective index material were varied. The thickness of the effective index layer was also iteratively adjusted. The best fit of the two curves (Fig. 9) was obtained for an effective index layer thickness of 31 nm and an effective index of $n_{eff} = 0.52 + 4.3j$, at a wavelength of 630 nm. This refractive index is quite different from indices of any known metals that can be used for SPR excitation in a continuous layer configuration.

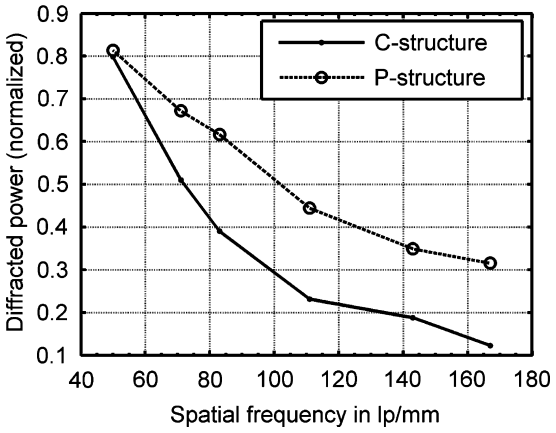

Fig. 8. Modulation transfer function obtained for the two simulated structures.

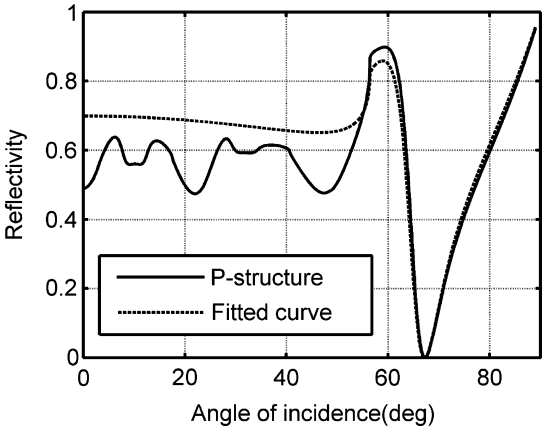

Fig. 9. Comparison of the SPR curves for the P-structure (patterned silver layer) and C-structure with an effective index material.

5. Conclusions

RCWA and FDTD-based computer simulations of SPR-based SLM with LC, as the programmable index material, were performed. It was shown that the spatial resolution of the device can be improved by optimizing the metal layer supporting the SPs. A fine, small-scale patterning of the metal layer was analyzed as a possible way to effectively change the complex refractive index of the SPs supporting layer thereby allowing an increased resolution. At high spatial frequencies (>80 lp/mm) a nearly two-fold improvement in the spatial resolution is achieved. The MTF obtained from simulations with real LC indicates that the fringing field shows little effect on the device performance.

The resolution improvement using patterned metal layer is attributed to the modification of the effective refractive index of the patterned metal layer, relative to that of the continuous, non-patterned metal. Further improvement of spatial resolution can be achieved by a careful choice of patterned metal parameters (patterning pitch, groove width and shape).

Acknowledgment

The partial support of this work by the Israel Science Foundation (ISF) is gratefully acknowledged.

References

[1] H. Raether, Phys. Thin Films 9 (1977) 145.
[2] H. Raether, Surface Plasmons, Springle, Berlin, 1988.
[3] K. Welford, Opt. Quantum Electron. 23 (1991) 1.
[4] J. Homola, Anal. Bioanal. Chem. 377 (2003) 528.
[5] J. Homola, S.S. Yee, G. Gauglitz, Sens. Actuators, B 54 (1999) 3.
[6] R.D. Harris, J.S. Wilkinson, Sens. Actuators, B 29 (1995) 261.
[7] K.A. Tetz, L. Pang, Y. Fainman, Opt. Lett. 31 (2006) 1528.
[8] I.R. Hooper, J.R. Sambles, Appl. Phys. Lett. 85 (2004) 3017.
[9] I.R. Hooper, J.R. Sambles, J. Appl. Phys. 96 (2004) 3004.
[10] E. Yeatman, E.A. Ash, Electron. Lett. 23 (1987) 1091.
[11] B. Rothenhausler, W. Knoll, Nature 332 (1988) 615.
[12] C.E.H. Berger, R.P.H. Kooyman, J. Greve, Rev. Sci. Instrum. 65 (1994) 2829.
[13] E.M. Yeatman, Biosens. Bioelectron. 11 (1996) 635.
[14] E. Fu, J. Foley, P. Yager, Rev. Sci. Instrum. 74 (2003) 3182.
[15] M.G. Somekh, S. Liu, T.S. Velinov, C.W. See, Appl. Opt. 39 (2000) 6279.
[16] H.E. de Bruijn, R.P.H. Kooyman, J. Greve, Appl. Opt. 32 (1993) 2426.
[17] U. Fernandez, T.M. Fischer, W. Knoll, Opt. Commun. 102 (1993) 49.
[18] E.M. Yeatman, M.E. Caldwell, Appl. Phys. Lett. 55 (1989) 613.
[19] M.E. Caldwell, E.M. Yeatman, Electron. Lett. 27 (1991) 1471.
[20] M.E. Caldwell, E.M. Yeatman, Appl. Opt. 31 (1992) 3880.
[21] T. Okamoto, T. Kamiyama, I. Yamaguchi, Opt. Lett. 18 (1993) 1570.
[22] C. Jung, S. Yee, K. Kuhn, Appl. Opt. 34 (1995) 946.
[23] K.H.F. Chiang, S.T. Wu, S.H. Chen, Jpn. J. Appl. Phys. 41 (2002) 4577.
[24] B. Apter, U. Efron, E. Bahat-Treidel, Appl. Opt. 43 (2004) 11.
[25] U. Efron, B. Apter, E. Bahat-Treidel, J. Opt. Soc. Am. A 21 (2004) 1996.
[26] Grating Solver Development Company, GSOLVER software, <http://www.gsolver.com/products/index.html>.
[27] Optiwave corporation, OptiFDTD software, <http://www.optiwave.com/site/products/fdtd.html>.
[28] Autronics-Melchers, 2dimMOS software, <http://www.autronic-melchers.com/index.php>.
[29] J.R. Sambles, G.W. Bradbery, F. Yang, Contemp. Phys. 32 (1991) 173.
[30] A.D. Rakic, A.B. Djurisic, J.M. Elazar, M.L. Majewski, Appl. Opt. 37 (1998) 5271.
[31] C.V. Brown, Em.E. Kriezis, S.J. Elston, J. Appl. Phys. 91 (2002) 3495.
[32] A. Tanone, S. Jutamulia, Liquid-crystal spatial light modulators, in: F.T.S. Yu, S. Jutamulia (Eds.), Optical Pattern Recognition, Cambridge University Press, 1998.
[33] H. De Smet, J. Van den Steen, A. Van Calster, SID Symp. Digest Techn. Pap. 32 (2001) 968.